UC Irvine
UC Irvine Previously Published Works

Title
Evolution of particle-laden jet flows - A theoretical and experimental study

Permalink
https://escholarship.org/uc/item/9469j8h0

Journal
AIAA Journal, 27(2)

ISSN
0001-1452

Authors
Mostafa, AA
Mongia, HC
McDonell, VG
et al.

Publication Date
1989

DOI
10.2514/3.10079

Peer reviewed

Evolution of Particle-Laden Jet Flows: A Theoretical and Experimental Study

A. A. Mostafa* and H. C. Mongia†
General Motors Corporation, Indianapolis, Indiana
and
V. G. McDonell‡ and G. S. Samuelsen§
University of California, Irvine, California

A combined experimental/analytical investigation is being conducted to study the interaction of particles and turbulent fluid flowfields under a wide range of test conditions. As a first step, the developing region of an unconfined axisymmetric turbulent jet with and without glass beads of 105 μm diam (d) has been addressed for two mass loading ratios, $LR = 0.2$ and 1.0. A well-defined data set suitable for the validation of two-phase flow models was obtained by using a two-component phase Doppler technique. The theoretical calculations, based on a stochastic Lagrangian treatment along with a two-equation turbulence model for two-phase flows, yield reasonable and encouraging agreement with the measurements.

Nomenclature

$c_\mu, c_{\epsilon 1}, c_{\epsilon 2}, c_{\epsilon 3}$	= coefficients in the turbulent model
c_D	= drag coefficient
d	= particle diameter
D	= nozzle diameter
F	= interphase friction coefficient
g	= gravitational acceleration
K	= kinetic energy of turbulence
ℓ_e	= eddy size
m	= particle mass
N	= number of particles represented by the trajectory k
$\dot{n}$	= particle number density
P	= static pressure
r	= distance in the radial direction
Re	= Reynolds number
t_i, t_0	= times when the particle enters and leaves the carrier-phase control volume
$U, u, \tilde{U}$	= mean, fluctuating, and instantaneous velocity of the carrier phase
$V, v, \tilde{V}$	= mean, fluctuating, and instantaneous velocity of the particles
z	= distance in the axial direction
ΔV	= control volume used in the carrier-phase solution
ϵ	= kinetic energy dissipation rate
μ	= dynamic viscosity of the carrier phase
ν_t	= kinematic eddy viscosity of the carrier phase
ρ	= material density
τ_d	= particle dynamic relaxation time
τ_e	= turbulent eddy lifetime
τ_L	= carrier-phase Lagrangian time scale
τ_r	= residence time of the particle in the eddy
$\sigma_k, \sigma_\epsilon$	= coefficients in the turbulence model
ϕ	= volume fraction

Subscripts

0	= conditions at the nozzle exit
1	= carrier phase
2	= dispersed phase
c	= conditions at the jet centerline
i	= ith direction
r	= radial direction
z	= axial direction
Θ	= azimuthal direction

Superscripts

k	= kth trajectory of a computational particle

Abbreviations

DT	= deterministic treatment
LR	= mass flow rate of the particles compared with that of air at the nozzle exit
ST	= stochastic treatment

I.   Introduction

TO facilitate the development of analytical design methodology for future advanced gas turbine combustion systems, improved physicochemical combustion models need to be formulated and validated with data from well-conceived experimental configurations. Currently, an experimental/analytical study is being conducted to enhance the understanding of the fuel-spray interaction with the turbulent swirling recirculating flow in a simulated axisymmetric combustor without reaction. The first step of this study concerns the developing region of unconfined turbulent axisymmetric jets with and without particles. The particle-laden jet was selected as a fundamental case because the single-phase jet turbulence models are reasonably well developed so that the important issues can be addressed in regard to particle dynamics and interaction between the two phases. Moreover, this type of flow provides well-defined initial conditions for both phases.

Most previous measurements[1-3] in particle-laden jets focused on the effects of the dispersed phase on the gas-flow properties. Very little information regarding particle quantities is reported. Others[4-7] have made measurements of both
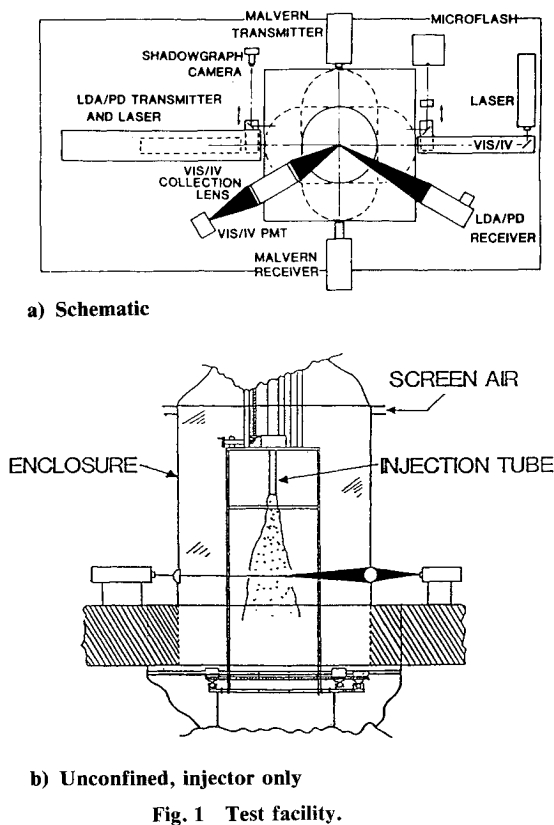
*Senior Engineering Associate, Allison Gas Turbine Division.
†Chief, Combustors, Allison Gas Turbine Division.
‡Research Assistant, Combustion Laboratory, Department of Mechanical Engineering.
§Professor, Combustion Laboratory, Department of Mechanical Engineering.

a) Schematic

b) Unconfined, injector only

Fig. 1   Test facility.

a) Before air classification

b) After air classification

Fig. 2   Glass-bead distribution before and after air classification.

phases but do not report the inlet conditions needed for the development of a reliable mathematical model. More recently, detailed measurements were performed[8,9] to provide considerably more information about the two phases but were mainly concerned with the fully developed flow region. The present investigation differs from these previous studies in many details, but principally in providing as much information as possible about the mean and turbulent quantities for the two phases in the jet developing region $(z/D \leq 12.5)$, which is of primary interest in gas turbine applications.

The acquisition of data in two-phase flows has to date been restricted by the limitations of instrumentation. Size and velocity data have been determined, for example, by either the tedious means of double-pulse imaging or by means of hybrid light scatter and laser-doppler anemometry techniques. The current effort uses a relatively new method, phase/Doppler interferometry, which provides point measurements of both particle size and particle velocity. The particle-size measurement allows discrimination between particle velocities (105 μm in the present case) and gas-phase velocities as represented by micron-sized "seed" particles.

A number of two-phase models are currently employed, namely, the two-fluid[10-12] and the discrete droplet models.[13-15] For a description, discussion of limitations, and computer cost of these two models, the reader is referred to the reviews of Crowe,[13] Sirignano,[16] and the recent work of Mostafa and Mongia.[17] The discrete droplet model that uses an Eulerian description of the fluid field and a Lagrangian formulation for particle motion was selected in the present study. An important component of the latter formulation is the manner in which the effects of gas turbulence on particle dispersion are simulated. In many studies,[18,19] this effect was entirely ignored (deterministic treatment),[9] whereas others[20,21] introduced an effective velocity or diffusion force to model the particle diffusional effects caused by gas turbulence. This force depends on the particle concentration gradient and an effective diffusion coefficient. The relevant reliable experimental information is not available to test the accuracy of the diffusion-force approach. A third and probably more accurate approach is the simulation of the diffusion directly, as a random walk of
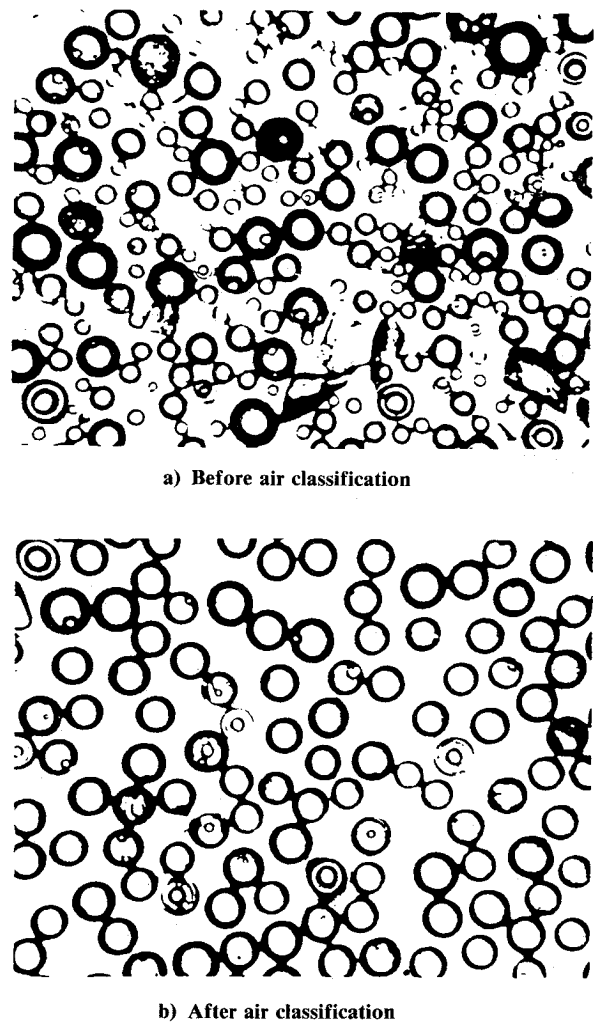
the particles acted on by the turbulent gas velocity field. This stochastic rather than deterministic approach has been recommended by many workers.[9,14] In the present study, the performance of the stochastic and deterministic treatments against the experimental data is elucidated.

The presence of dispersed particles causes a significant change in the turbulence structure of the carrier phase.[3,8,9,12] Because of the fluctuating velocity of the particles relative to the gas, a reduction in the gas turbulence kinetic energy and an increase in its dissipation rate generally occurs. This effect is simulated in the present study by introducing extra terms in the modeled equations of turbulent kinetic energy and its dissipation rate.[17]

The main objectives of this paper are 1) to provide a benchmark quality data set for the mean and rms quantities in the developing region of a single-phase jet, and a particle-laden jet with two mass loading ratios, and 2) to evaluate the theoretical calculations of two-phase models against the experimental data.

Section II provides a description of the experimental test facility, diagnostics, and the glass beads, followed by a model description in Sec. III and numerical solution in Sec. IV. The comparison between measurements and predictions is presented in Sec. V, and conclusions are presented in Sec. VI.

II.   Experiment

Test Facility

A testing facility (Fig. 1) was designed to characterize a wide variety of flows under isothermal conditions. For the present
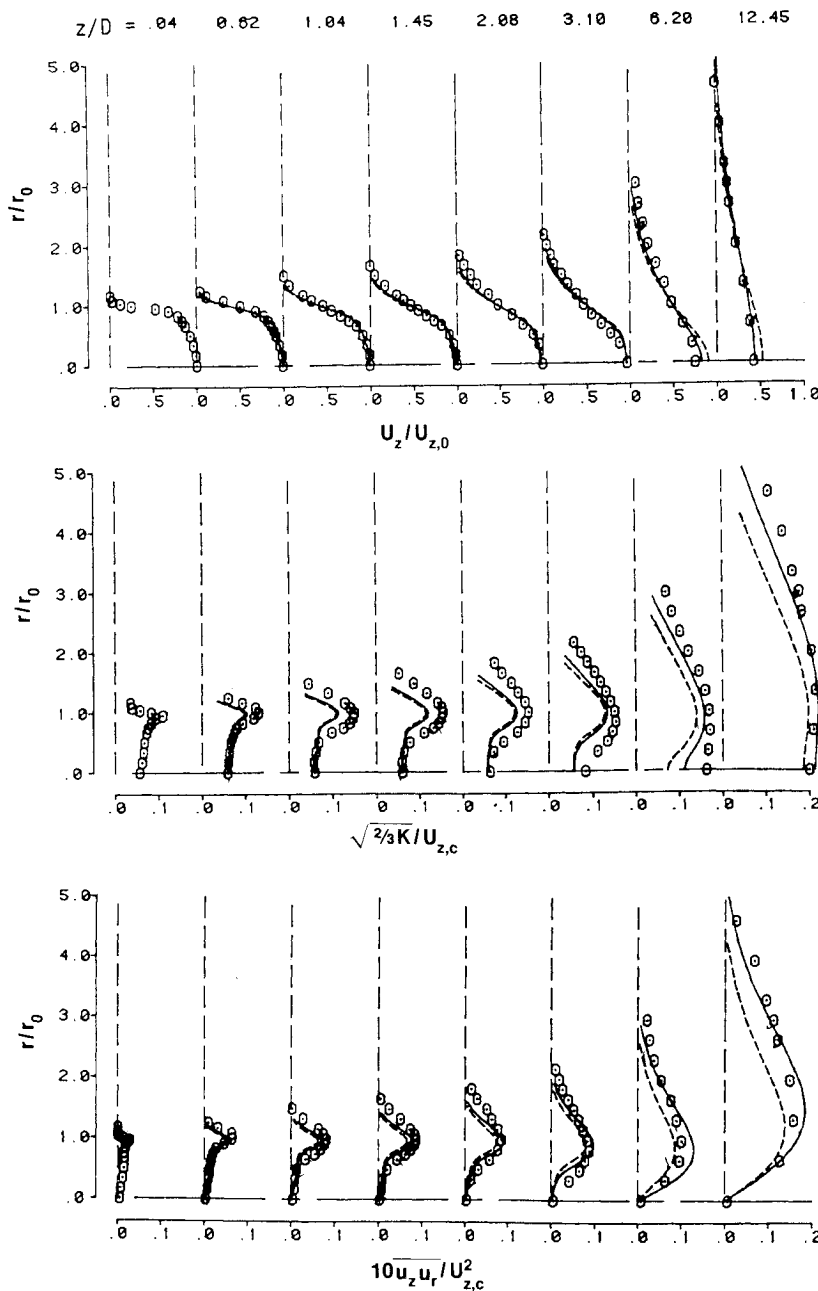
Fig. 3 Radial profiles of normalized mean axial velocity, turbulence kinetic energy, and shear stress for the single-phase jet; - - - standard model, —— modified model.

study, an unconfined flow configuration was selected, operating with a glass-bead injector (D = 25.3 mm i.d.) with no inlet swirl, as shown in Fig. 1b. In this configuration, the injector was directed downward within a 457-mm-square cage assembly. This entire assembly was surrounded by a Plexiglas and flexible plastic enclosure, which serves two primary purposes. First, the enclosure eliminates the effects of room air currents. Second, the enclosure permits a controlled amount of seeded air to be placed into the air that is entrained by the various flows, thus permitting accurate measurements in the jet outer region. The same quantity of air that was injected was removed via an exhaust system located at the bottom of the support cage. The support cage was mounted to the optics table from below via a two-axis traverse system. In addition, the injector was mounted onto a vertical traverse to provide a third degree of freedom. All positioning was monitored via a three-axis digital indicator, which permits positioning to within 0.01 mm. Data were obtained at seven axial stations: 15, 25, 35, 50, 75, 150, and 300 mm from the exit plane of the injector. In addition, measurements were made at the exit plane to provide initial conditions (Table 1). At each axial station, measurements were conducted at between 10 and 20 radial points.

Diagnostics

A two-component phase Doppler system (Aerometrics, Inc., Model 2100-3) was used to map out the flowfield for both phases. The instrument simultaneously measures size and two orthogonal components of velocity for individual particles.[22] The technique has been evaluated using both laser diffraction and laser visibility techniques in a series of studies.[23,24] Using the experimental setup described, three components of mean and fluctuating velocities and two components of Reynolds stress were measured for the two phases. To distinguish both directions of flow, frequency shifting was provided by rotating gratings.

Discrimination of phases or of different-sized beads was inherent in the operation of the system. By sizing all particles, statistics are generated for both phases. Aluminum oxide (nominal 2.0 μm) was used to seed the gas phase and, when sized, provides a local peak in size scores substantially less than the local peak for the beads.

Table 1   Experimental flow conditions at 0.04D downstream of pipe exit[a]

Parameter	Single-phase jet	Particle-laden jet	
		Case 1	Case 2
Gas-phase (air)			
Centerline velocity $U_{z,0}$, m/s	4.74	4.70	4.20
Density ρ_1, kg/m^3	1.178	1.178	1.178
Mass flow rate m_1, kg/s	0.0021	0.0021	0.0021
Reynolds number $Re = 4m_1/\pi\mu_1 D$	5712	5712	5712
Particle-phase (glass beads)			
Centerline velocity $V_{z,0}$, m/s		4.41	3.39
Density ρ_2, kg/m^3		2500.0	2500.0
Mass flow rate m_2, kg/s		0.00042	0.0021
Ratio of particle-to-gas mass flow rate, LR		0.2	1.0

[a]$D = 0.0253$; inlet profiles of mean and fluctuating velocities and particle number density are plotted in Figs. 3–12.

Glass Beads

To obtain a suitably narrow size distribution for the glass beads, several steps were taken. Beads provided by the manufacturer, though stated to have a narrow size range, were unacceptable due to a large quantity of shards, irregular beads, and small satellite beads. Air classification (a separation technique based upon particle size and weight) of the beads provided a much more uniform distribution, as shown in Fig. 2. The actual size of the air-classified beads were determined by microscope to be 100–110 μm. This resulting narrow size range provides for 1) better representation of a monodispersed nonevaporating spray, and 2) better discrimination by the phase/Doppler. The size distributions measured by the phase/Doppler were not expected to reflect those indicated by inspection through the microscopes due to internal bubbles (see Fig. 2) and slight asphericities.[25] It is noteworthy that the mean size measured by the phase/Doppler falls within the minimum and maximum values determined under the microscope.

Data Sets

Data are tabulated and the experiment is documented in Ref. 26, following the format outlined in Ref. 27.

III.   Theoretical Methods

It is assumed that the particles are sufficiently dispersed so that particle-particle interaction is negligible. This assumption restricts the present study to dilute particulate suspensions. It is also assumed that the mean flow is steady and the material properties of the two phases are constant.

The equations of motion for the particles are cast in the Lagrangian form, whereas the carrier-phase transport equations are formulated following the Eulerian treatment. The governing equations of the two phases are coupled primarily by the momentum interchange and the extra energy dissipation due to the relative velocity fluctuation between the gas and particles. In the following paragraphs, the governing transport equations for particle-laden jet flows are briefly described.

Particle Equations

The discrete particle approach is considered in this study. As such, the dispersed phase is represented by computational particles rather than a continuous distribution function.[16] This amounts to a statistical (Monte Carlo) formulation of the problem, since a finite number of particles is used to represent a very large number of particles present in the field. Each of these computational particles characterizes a group of physical particles possessing the same characteristics, such as size, velocity, and temperature.

For large particle-to-gas density ratio, the only important forces on a particle are the inertia, drag, and gravity, in which

case the equation of motion of the kth computational particle in the ith direction[9,14] is

$$\frac{d\tilde{V}_i^k}{dt} = \frac{(\tilde{U}_i - \tilde{V}_i^k)}{\tau_d} + g_i \quad (1)$$

where

$$\tau_d = \frac{4d^k \rho_2}{3C_D \rho_1 \, |\tilde{U} - \tilde{V}^k|} \quad (2)$$

and

$$\tilde{U}_i = U_i + u_i$$

The particles are assumed spherical so that the experimental results for the drag coefficient of a solid sphere can be used. For a moderate Reynolds number, $1 < Re^k < 260$, the drag coefficient is given by[28]

$$C_D^k = (24/Re^k)(1 + 0.1315 \, [Re^k]^{0.82 - 0.05w})$$
$$0.01 < Re^k \le 20 \quad (3)$$

$$C_D^k = (24/Re^k)(1 + 0.1935 \, [Re^k]^{0.6305})$$
$$20 < Re^k < 260 \quad (4)$$

where $w = \log_{10} Re^k$, and the particle Reynolds number is calculated from

$$Re^k = \rho_1 |\tilde{U} - \tilde{V}^k| d^k / \mu_1 \quad (5)$$

where

$$|\tilde{U}| = \sqrt{\Sigma \tilde{U}_i^2} \quad (6)$$

$$|\tilde{V}^k| = \sqrt{\Sigma (\tilde{V}_i^k)^2} \quad (7)$$

The particle location at any instant of time is determined from

$$\frac{dx_i^k}{dt} = \tilde{V}_i^k \quad (8)$$

In Eq. (1), $\tilde{U}_i$ is obtained from the solution of the mean flow equations of the carrier phase. Consistent with the use of the K-ϵ model for the carrier phase, u_i is chosen randomly from an isotropic Gaussian distribution with mean square deviation $\frac{2}{3} K$. Subsequently, after each elapsed time equal to turbulent characteristics time τ, a new value for u_i is chosen. τ is the minimum of turbulent eddy lifetime (τ_e) and the residence time of the particle in the eddy[14] (τ_r). It is assumed that the characteristic length of the turbulent eddies is that of the dissi-

pation length scale ℓ_e, given by

$$\ell_e = c_\mu^{3/4} K^{3/2}/\epsilon \qquad (9)$$

The eddy lifetime is obtained from

$$\tau_e = \ell_e/u_i \qquad (10)$$

The residence time of the particle in the eddy, e.g., the time for a particle to pass through that eddy, is estimated from

$$\tau_r = \ell_e/|\bar{U} - \bar{V}^k| \qquad (11)$$

Hence,

$$\tau = \min{(\tau_e, \tau_r)} \qquad (12)$$

For each particle, the equation of motion is integrated over as many time increments as required for the particle to traverse the required distance. When a sufficiently large number of particles is tracked, their averaged behavior should represent the cloud and yield the effects of the gas turbulence characteristics on the motion of the particles.

The carrier-phase momentum source per unit volume resulting from all particle trajectories is obtained as follows[17]:

$$S_i = \sum_k \frac{Nm^k(U_i - V_i^k)}{\Delta V \, \tau_d} = \sum_k F^k \phi^k (U_i - V_i^k) \qquad (13)$$

The volume fraction of the particles is given by

$$\phi^k = N \frac{\pi (d^k)^3}{6\Delta V} \qquad (14)$$

where

$$F^k = \frac{3\rho_1}{4d^k} C_D^k \, |U - V^k| \qquad (15)$$

Carrier-Phase Equations

The governing equations of the carrier phase to be presented here are based on the model of Elghobashi et al.[12] and Mostafa and Mongia.[17] That model was devised for isothermal, nonreacting, dilute gas-particle turbulent shear flows and was presented in its general form using Cartesian tensor notations.[12] The modeled mean equations in the cylindrical coordinates for axisymmetric jet flow are presented below:

$$\rho_1 U_{z,z} + (\rho_1/r)(rU_r)_{,r} = 0 \qquad (16)$$

$$\rho_1 U_z U_{z,z} + \rho_1 U_r U_{z,r} =$$

$$-P_{,z} + \frac{1}{r}(\rho_1 r \nu_t U_{z,r})_{,r} - \sum_k \phi^k F^k (U_z - V_z^k) \qquad (17)$$

$$\rho_1 U_z U_{r,z} + \rho_1 U_r U_{r,r} =$$

$$-P_{,r} - \sum_k \phi^k F^k (U_r - V_r^k) - \frac{2}{3}\frac{\rho_1}{r}(rK)_{,r} \qquad (18)$$

In Eqs. (16-18), the comma-subscript notation indicates differentiation with respect to the spatial coordinates z and r. The kinematic eddy viscosity of the carrier phase is given by the following:

$$\nu_t = c_\mu(K^2/\epsilon) \qquad (19)$$

The modeled equations of the turbulence model for two-phase flows are given by[17]

$$\rho_1 U_z K_{,z} + \rho_1 U_r K_{,r} = \rho_1 \nu_t U_{z,r} U_{z,r} + \frac{1}{r}\left(\rho_1 \frac{\nu_t}{\sigma_k} rK_{,r}\right)_{,r}$$

$$-\rho_1 \epsilon - \sum_k 2KF^k \phi^k \left(1 - \frac{\tau_L}{\tau_L + \tau_D}\right) \qquad (20)$$

$$\rho_1 U_z \epsilon_{,z} + \rho_1 U_r \epsilon_{,r}$$

$$= c_{\epsilon 1} \frac{\epsilon}{K} [\rho_1 \nu_t U_{z,r} U_{z,r}] + \frac{1}{r}\left(\rho_1 r \frac{\nu_t}{\sigma_\epsilon} \epsilon_{,r}\right)_{,r} - c_{\epsilon 2} \rho_1 \frac{\epsilon}{K}$$

$$-c_{\epsilon 3}\frac{\epsilon}{K}\sum_k \left[2K \, F^k \phi^k \left(1 - \frac{\tau_L}{\tau_L + \tau_d}\right)\right] \qquad (21)$$

The carrier-phase Lagrangian time scale is given by[17]

$$\tau_L = 0.35K/\epsilon \qquad (22)$$

The values of the coefficients appearing in Eqs. (9-21) are $\sigma_k = 1.0$, $c_\mu = 0.09$, $\sigma_\epsilon = \frac{1}{3}$, $c_{\epsilon 1} = 1.44$, $c_{\epsilon 2} = 1.92$, and $c_{\epsilon 3} = 1.0$.

With this set of constants, the spreading rate for axisymmetric jet flows in the self-similar region is overpredicted by about 30%. This result led to the modification of two constants to be functions of the centerline velocity gradient, maximum velocity different across the layer, and the flow width as follows[29]:

$$c_\mu = 0.09 - 0.04f_1 \qquad (23)$$

$$c_{\epsilon 2} = 1.92 - 0.0067f_1 \qquad (24)$$

where

$$f_1 = 0.5R \left| \frac{\left|\dfrac{dU_{z,c}}{dz}\right| - \left|\dfrac{dU_{z,c}}{dz}\right|}{U_{z,c} - U_{z,\infty}} \right|^{0.2} \qquad (25)$$

where $U_{z,c}$ and $U_{z,\infty}$ are the axial velocities of the fluid at the jet centerline and the ambient stream, respectively, and R is the local jet width.

IV.   Numerical Solution

The carrier-phase governing equations are solved numerically using the marching finite-difference solution procedure of Spalding.[30] The present calculations were obtained using a fine grid with 100 cross-stream grid points and marching step sizes limited by 3% of the current radial grid width or an entrainment increase of 3%, whichever is smaller.

The ordinary differential equations governing particle motion are solved using a second-order finite-difference algorithm. Ten thousand particles are used for the stochastic treatment, whereas 200 particles are computed when the deterministic method is compared with the stochastic one.

V.   Results and Discussion

In all cases, computations commenced at a downstream distance of 0.04 nozzle diameter (1 mm from the nozzle exit) where measured mean and rms velocity profiles for both gas and particles are available. Consistent with the K-ϵ model, the initial profile for the turbulence energy dissipation rate was obtained in terms of the measured kinetic energy of turbulence, shear stress, and axial velocity gradient. The gas rms velocities were calculated by assuming $u_z^2 : u_r^2 : u_\theta^2 = K : K/2 : K/2$, which is well accepted for jet flows. The results are plotted in a dimensionless form vs r/r_0. In this way the jet
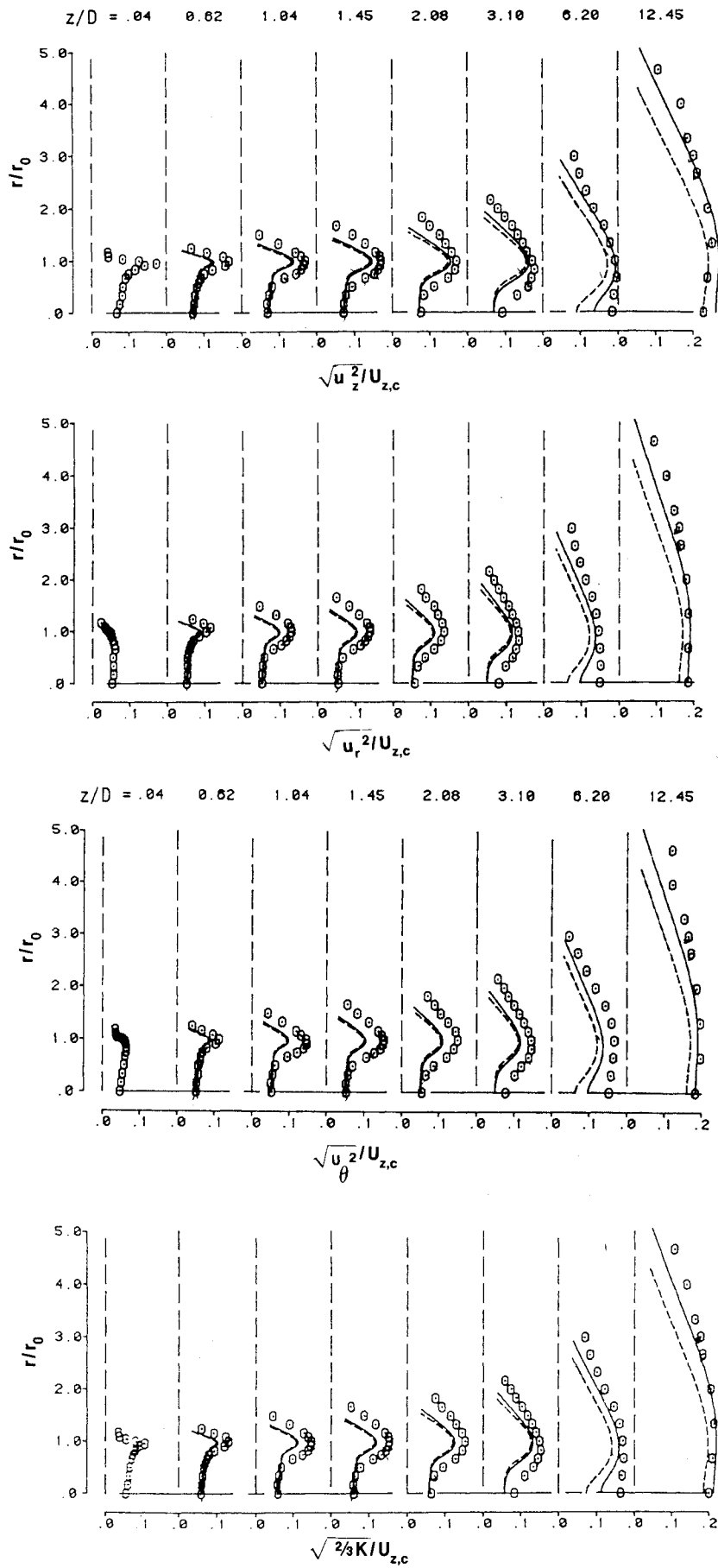
Fig. 4   Radial profiles of normalized rms velocity components and turbulence kinetic energy for the single-phase jet; - - - standard model, —— modified model.
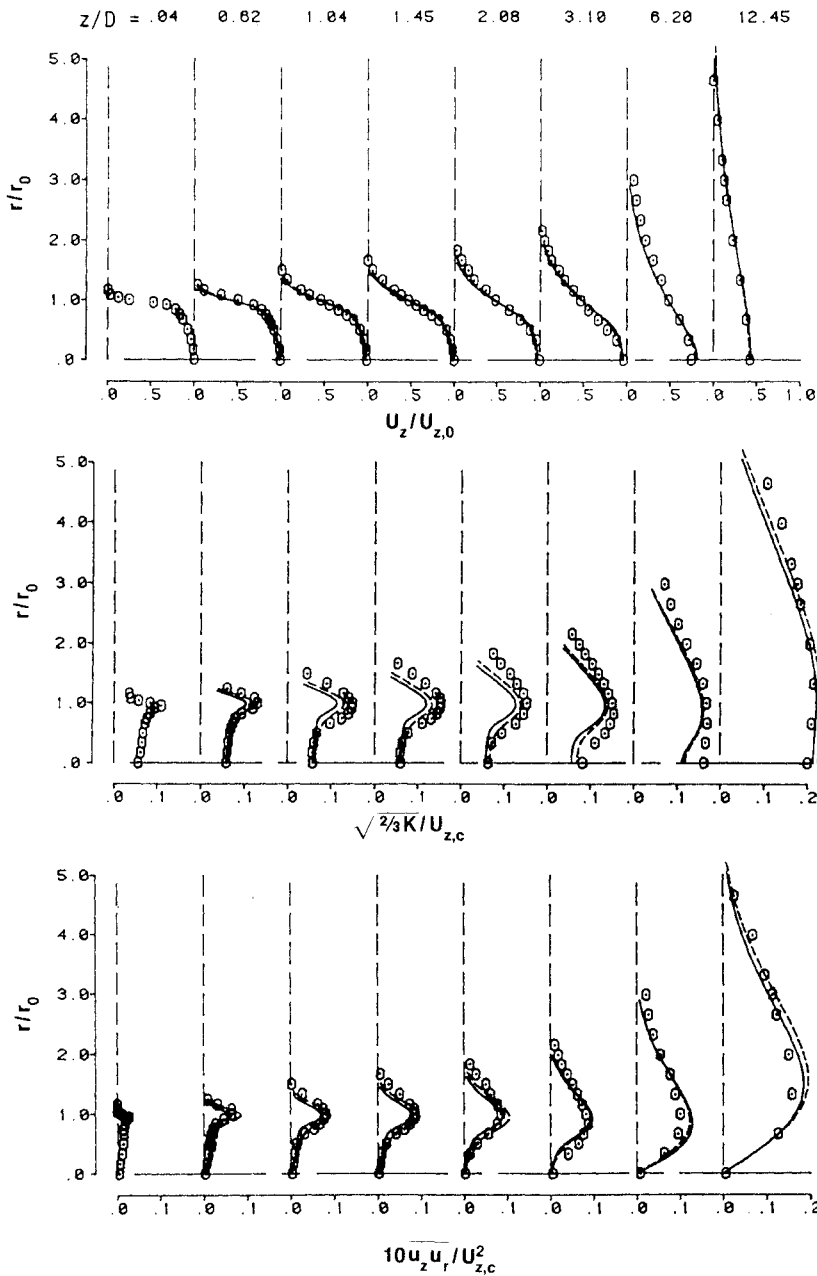
Fig. 5   Radial profiles of normalized mean axial velocity, turbulence kinetic energy, and shear stress for the single-phase jet; influence of initial ϵ; $---$ $\epsilon_{inlet} = \epsilon_0$, $\longrightarrow$ $\epsilon_{inlet} = 0.5\ \epsilon_0$.

spreading can be easily seen from the axial profiles of the mean axial velocities. All quantities except mean axial gas velocities are normalized by the local mean centerline velocity. The mean axial gas velocities are normalized by the initial jet centerline velocity at the nozzle exit, $U_{z,0}$, so that the jet centerline velocity decay can be illustrated in the same figure.

Single-Phase Jet

To establish a baseline for two-phase flow modeling, predictions of a single-phase fluid flowfield were first compared with data. The performance of the turbulence model in the jet developing region and the effect of the inlet dissipation rate on the predictions were assessed. Both the standard K-ϵ, and its modified version[30] for round jets were used. In the latter (hereafter referred to as modified K-ϵ), the effect of the centerline velocity gradient on c_μ and $c_{\epsilon 2}$ was allowed to obtain the correct spreading rate of self-similar round jets [see Eqs. (23) and (24)].

Figures 3 and 4 relate to the measurements of a single-phase jet and present comparisons with calculations using the two K-ϵ models. Figure 3 presents mean axial velocity, kinetic energy of turbulence (K), and shear stress, whereas Fig. 4 shows the three normal stresses and K. Both models yield

good overall agreement with measurements close to the nozzle exit, but for the region further downstream the standard model performs better. In the first region, the decay of the centerline velocity is very small; therefore, the two sets of model constants are quite the same. When the axial velocity started to decay substantially (at about $z/D = 5$), c_μ and $c_{\epsilon 2}$ of the modified model decrease to values that give the observed spreading rate for self-similar round jets. For instance, at $z/D = 7$, c_μ decreases to a value of 0.064, whereas $c_{\epsilon 2}$ becomes 1.87. These low values reduced the turbulent diffusion and hence the decay of the centerline velocity.

It is interesting to observe that the underpredicted values of the kinetic energy of turbulence by the modified model in the region $z/D \geq 6$ are consistent with the same behavior in the developing region. This performance of the modified model made us question the inlet conditions, especially the ϵ values. To settle this issue, calculations were made with the standard model but with two inlet dissipation levels as given by ϵ_0 and $0.5\epsilon_0$ (or $c_\mu = 0.045$ at the inlet plane), where ϵ_0 is the dissipation reference conditions obtained from the measured profiles of mean velocity, turbulent kinetic energy, and shear stress at $z = 1$ mm. As seen from Fig. 5, halving the inlet dissipation rate improves the predictions of the kinetic energy
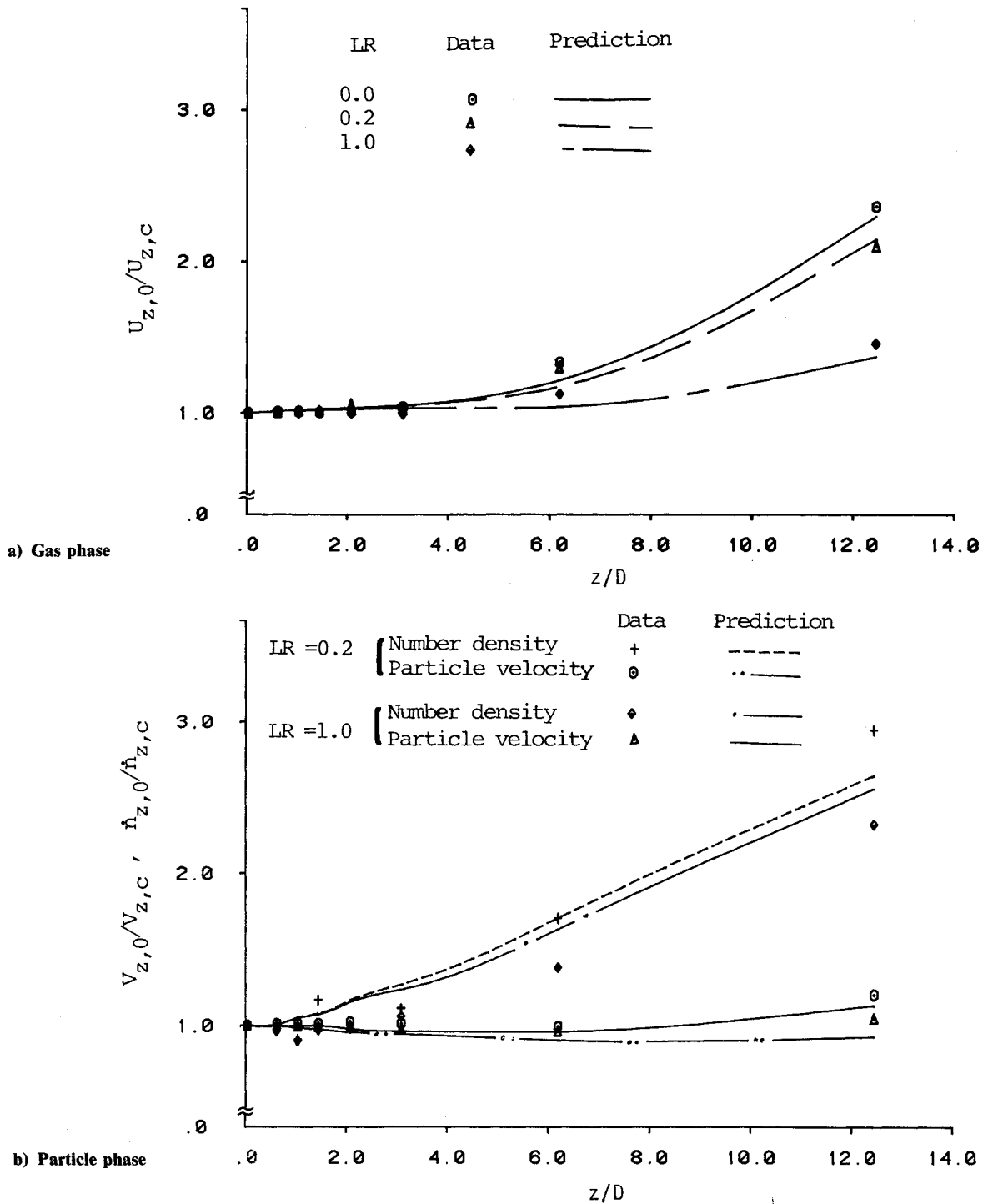

Fig. 6 Axial distribution of normalized centerline values of gas mean velocity, and particle mean velocity and number density.

of turbulence. This result prompted a repeat of the measurements at the three locations near the nozzle exit: at 1, 3, and 5 mm. The same values were obtained within experimental uncertainty.

In concluding this phase of the study, a decision was made as to which model would be used for two-phase flow modeling and what value of c_μ should be selected at the inlet plane. To maintain the empirical constants established by so many workers, c_μ at the inlet plane was initially taken as 0.09, and, since the comparison of the calculations with the two variants of the turbulence model indicates that the standard model agrees more closely with the measurements (especially for the mean axial velocity), it has been chosen as a basis for two-phase flow modeling.

Particle-Laden Jets

This section presents measured data and model predications for particle-laden jet flows. Two mass loadings, defined as the ratio of particle-to-gas mass flow rate at the inlet plane, $LR = 0.2$ and 1.0, were considered. To distinguish between the effects of mean and fluctuating gas velocity in particle transport, predictions using stochastic and deterministic treatments are compared with the measured data. The main difference between the two treatments is that the first considers the effect of gas turbulence on particle motion, whereas the second ignores it completely.

Figure 6 shows the measured and predicted (stochastic treatment) distributions of mean centerline velocities and particle number density normalized by their corresponding
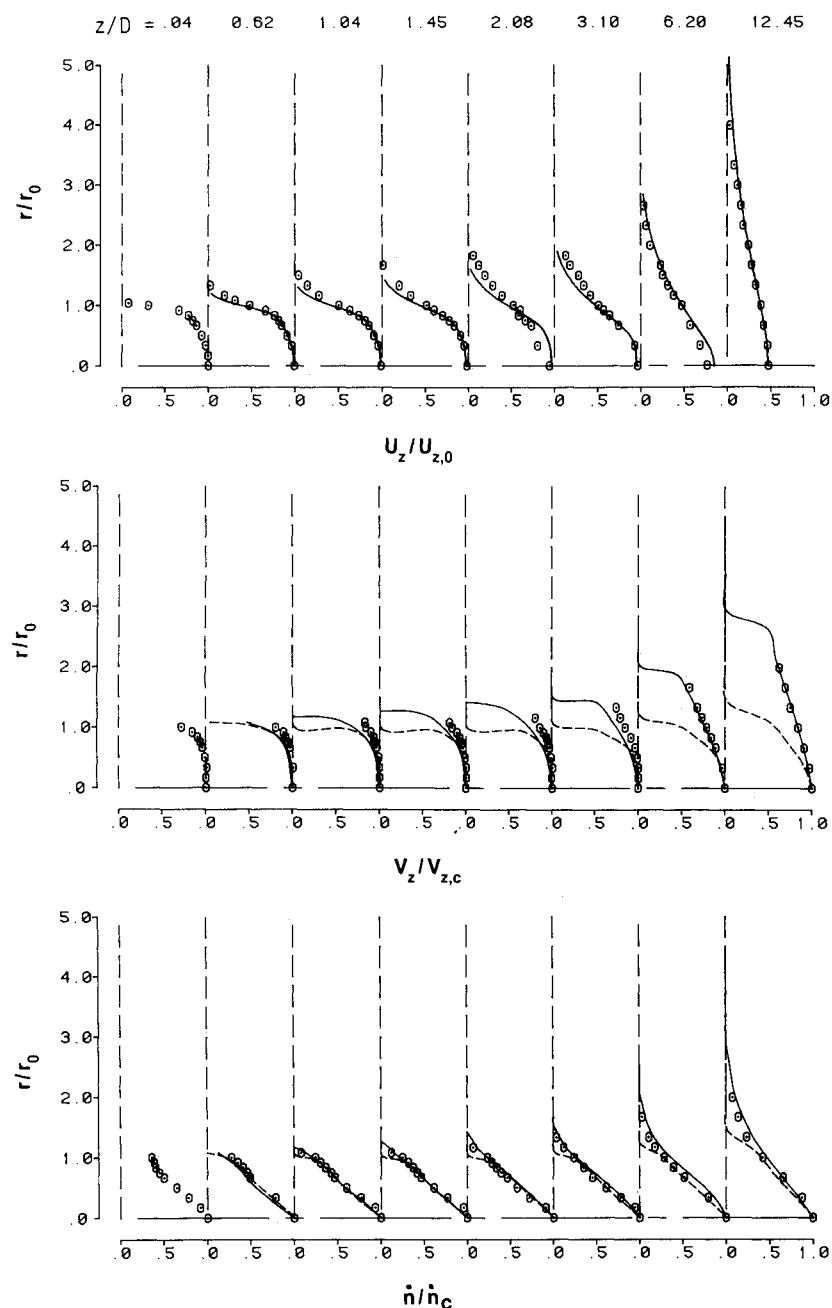
Fig. 7   Radial profiles of normalized gas axial velocity, particle axial and radial velocity components, and particle number density at loading ratio, LR = 0.2; - - - stochastic treatment, —— deterministic treatment.

values at the nozzle exit. Because of the slow decay of the particle mean velocity, there is a momentum transfer from the dispersed phase to the gas which causes an increase in the latter velocity compared with the corresponding single-phase values. This change in the gas-flow properties could also be attributed to the gas turbulence attenuation caused by particles. Gas turbulence attenuation causes a reduction in the jet spreading rate that results in less decay of the gas centerline velocity. Figure 6a shows a progressive increase in the gas centerline velocity with the particle loading ratio LR, which might be explained by the fact that both the momentum transfer and turbulence modulation are proportional to LR. It can be seen from Fig. 6b that the particle number density is decaying much faster than the particle velocity. This means that the spreading of the dispersed phase dilutes the particle concentration but does not necessarily decelerate the particles.

Figures 7-9 correspond to the measurements of a particle-laden jet with LR = 0.2 and indicate the extent to which the models described in Sec. III allow realistic calculations. Figure 7 presents the mean velocities of both phases and particle

number density whereas Figs. 8 and 9 show the rms values for the particles and gas and the shear stress of the latter. In the calculations, the turbulence model presented for two-phase flows was used. It can be seen from Fig. 7 that both stochastic (ST) and deterministic (DT) treatments yield nearly the same results for gas quantities. However, for particle quantities the ST provides good predictions compared with the experimental data, whereas the DT performs quite poorly for the particle flow properties. According to the latter, a particle moves radially due to its initial mean radial velocity and/or the mean radial gas velocity, both of which are very small compared with the axial component. This might explain the narrow distribution of particle mean axial velocity and number density predicted by the DT.

Figure 8 shows comparisons between predicted and measured values of gas turbulence kinetic energy and shear stress. It also presents the rms axial gas velocity and its corresponding value for the particles. If Fig. 8 is compared with Fig. 2, one could observe some reduction in the gas kinetic energy of turbulence caused by the particles. This phenomenon is more
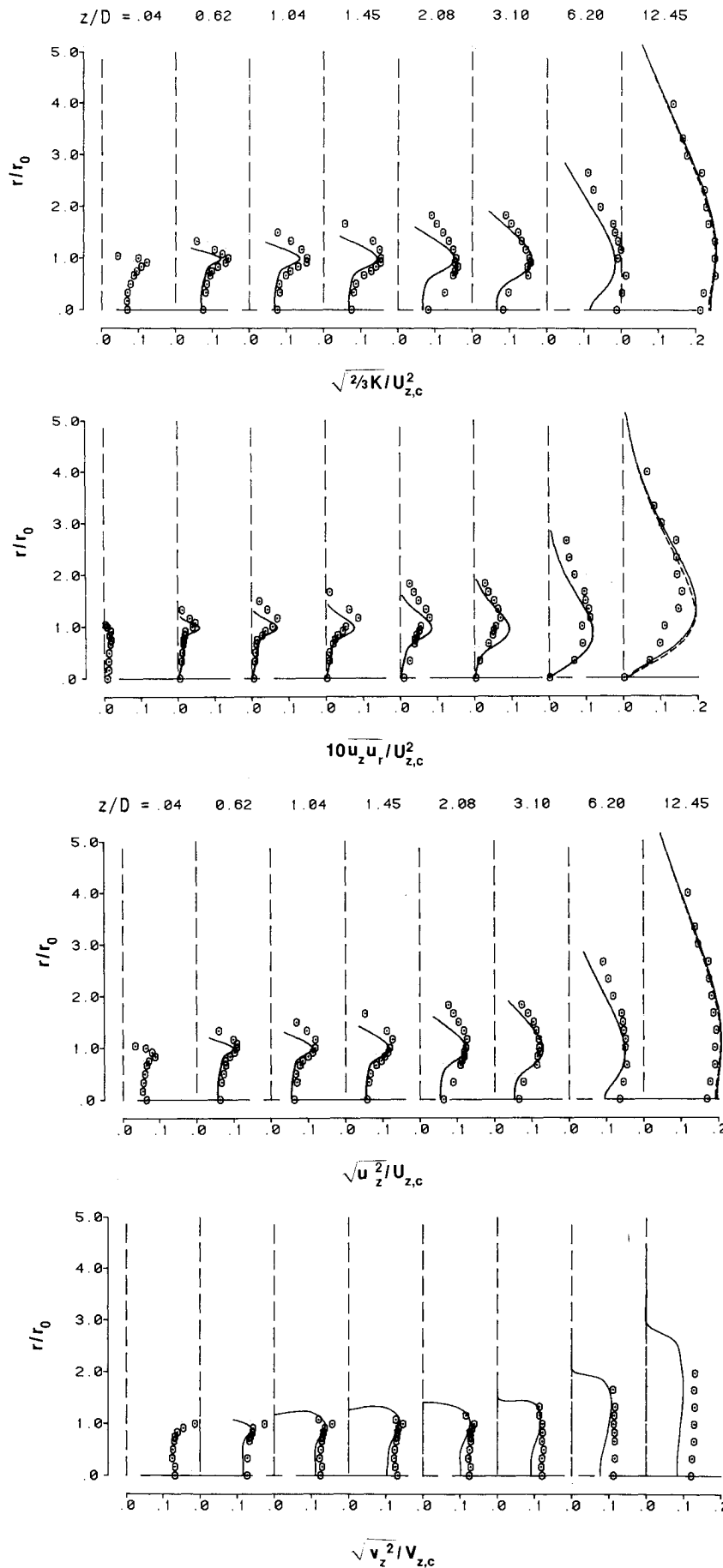
Fig. 8   Radial profiles of normalized gas turbulence kinetic energy, shear stress, and axial turbulence intensity, and particle axial turbulence intensity at loading ratio, LR = 0.2; - - - stochastic treatment, —— deterministic treatment.
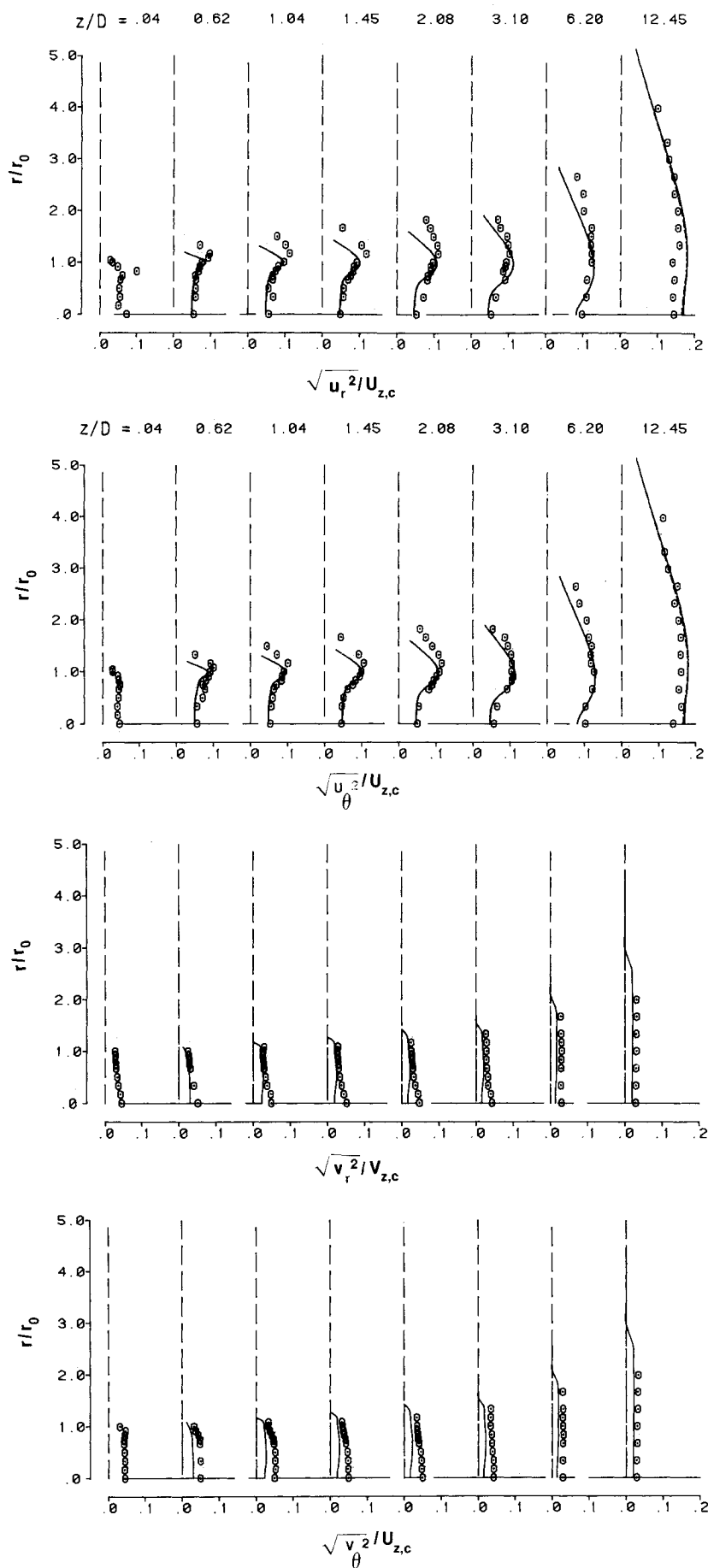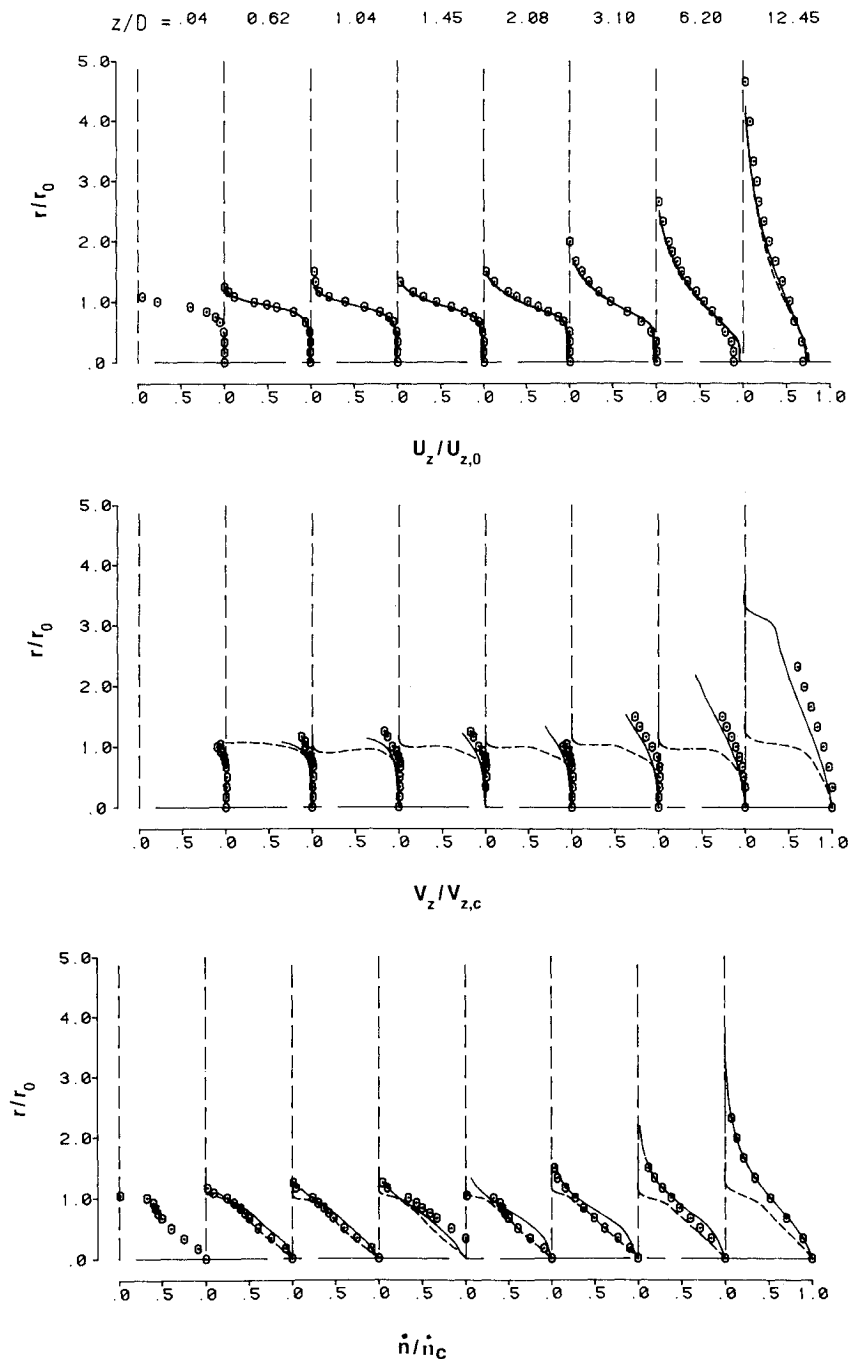
Fig. 9   Radial profiles of rms radial and azimuthal velocity components of gas and particles at loading ratio, LR = 0.2; – – – stochastic treatment, —— deterministic treatment.

Fig. 10 Radial profiles of normalized gas axial velocity, particle axial and radial velocity components, and particle number density at loading ratio, LR = 1.0; - - - stochastic treatment, —— deterministic treatment.

pronounced at LR = 1.0 and will be discussed below in connection with the results of that case. In Fig. 9, the comparisons are made for the radial and azimuthal rms velocities of both phases. It is seen that the ST predictions of rms particle velocities are in very good agreement with the data; v_z^2 is somewhat underpredicted near the jet centerline and overpredicted at the outer boundary. This is in agreement with the calculations of Shuen et al.[31] and Bulzan et al.,[32] who studied particle-laden jets under different flow conditions.

Figures 10-12 relate to the measurements of particle-laden jets at LR = 1.0 and present comparison with calculations. Figure 10 shows mean values for both phases, and Figs. 11 and 12 show the Reynolds stresses. It can be seen from these figures that the DT is inferior to the ST in predicting particle properties, the same behavior as observed at LR = 0.2, which could be attributed to the same physical reasonings discussed in connection with the results of that case.

By comparing Fig. 10 with Fig. 3, two effects of the particles on the gas mean axial velocity can be observed. First, the mean axial velocity profile at the inlet plane is flatter than the single-jet profile. This is due to the inlet profiles, which correspond to a fully developed pipe flow. (The injection tube diameter-to-length ratio was equal to 65.2.) At this condition, the particles are leading the fluid near the injector wall region and thus transfer momentum to the gas, which causes the flattening effect. Second, the mean axial gas velocity downstream of the injector is higher than the single-phase value. For instance, at $z/D = 12.45$, an increase of about 20% of the inlet single-phase velocity is caused by the presence of the particles. This phenomenon is explained in detail by Mostafa and Elghobashi[33] and can be attributed to two effects. One effect is the momentum transfer from the particles to the air, since V_z^k becomes greater than U_z after a short distance downstream from the injector. The other effect is the modulation of the gas turbulence caused by the particles.
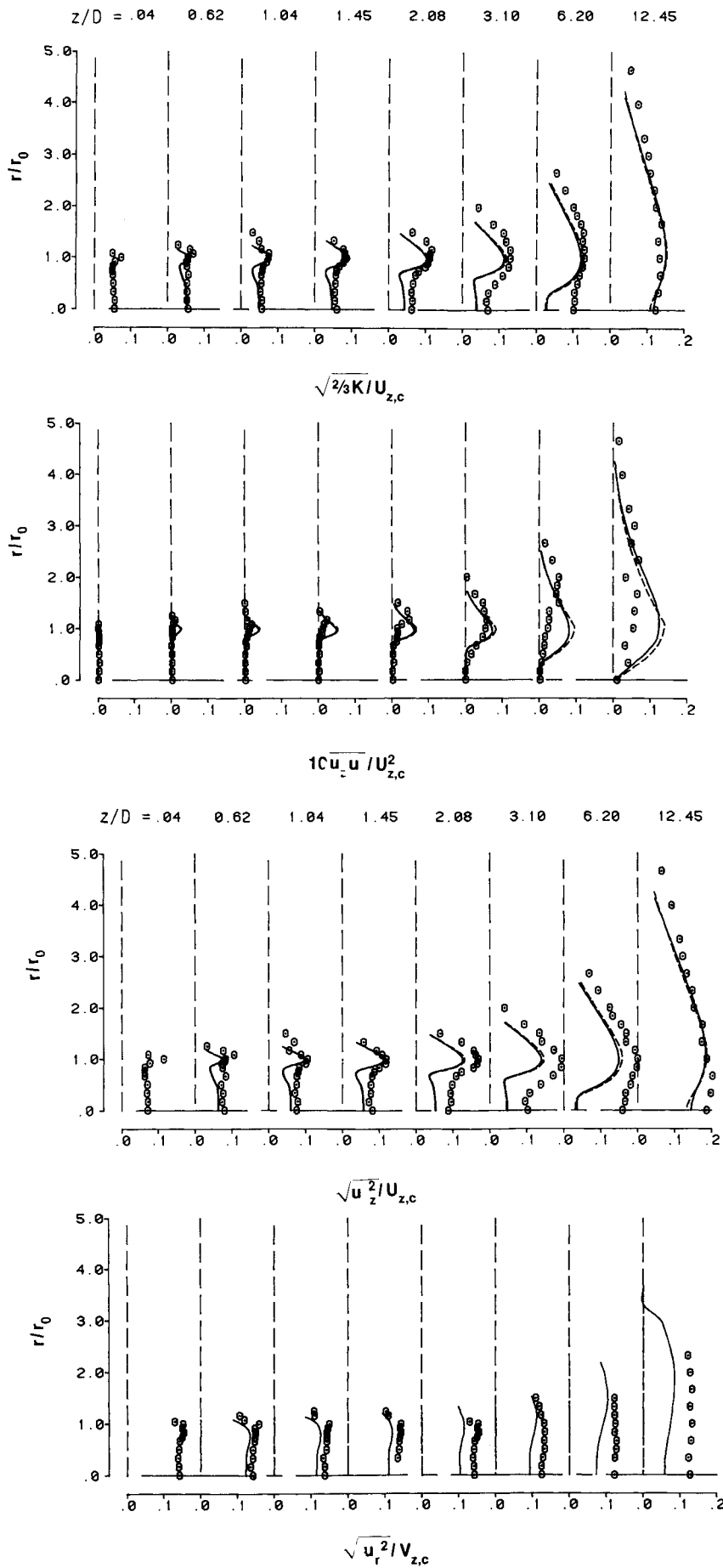
Fig. 11   Radial profiles of normalized gas turbulence kinetic energy, shear stress, and axial turbulence intensity, and particle axial turbulence intensity at loading ratio, LR = 1.0; - - - stochastic treatment, —— deterministic treatment.
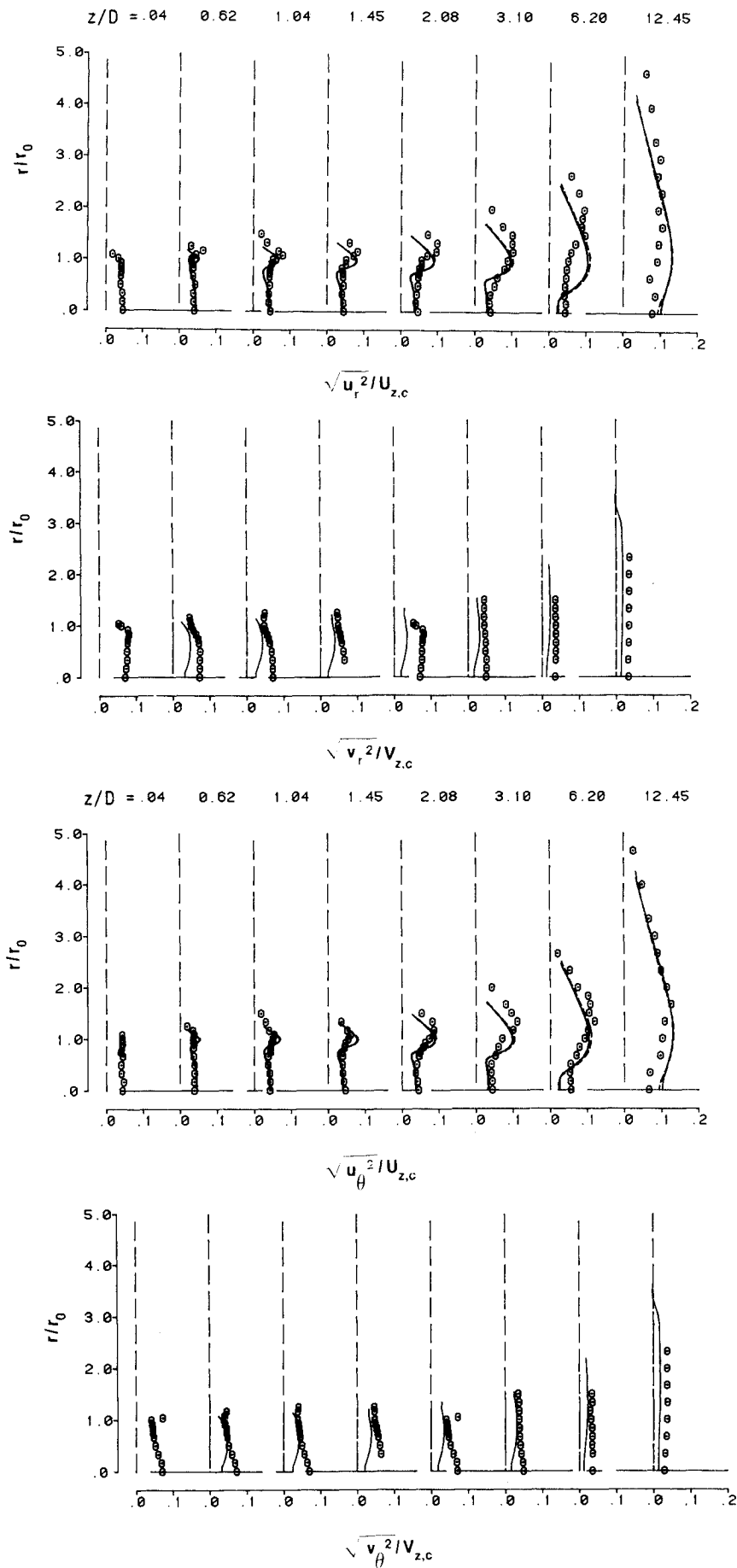
Fig. 12   Radial profiles of rms radial and azimuthal velocity components of gas and particles at loading ratio, LR = 1.0; - - - stochastic treatment, —— deterministic treatment.
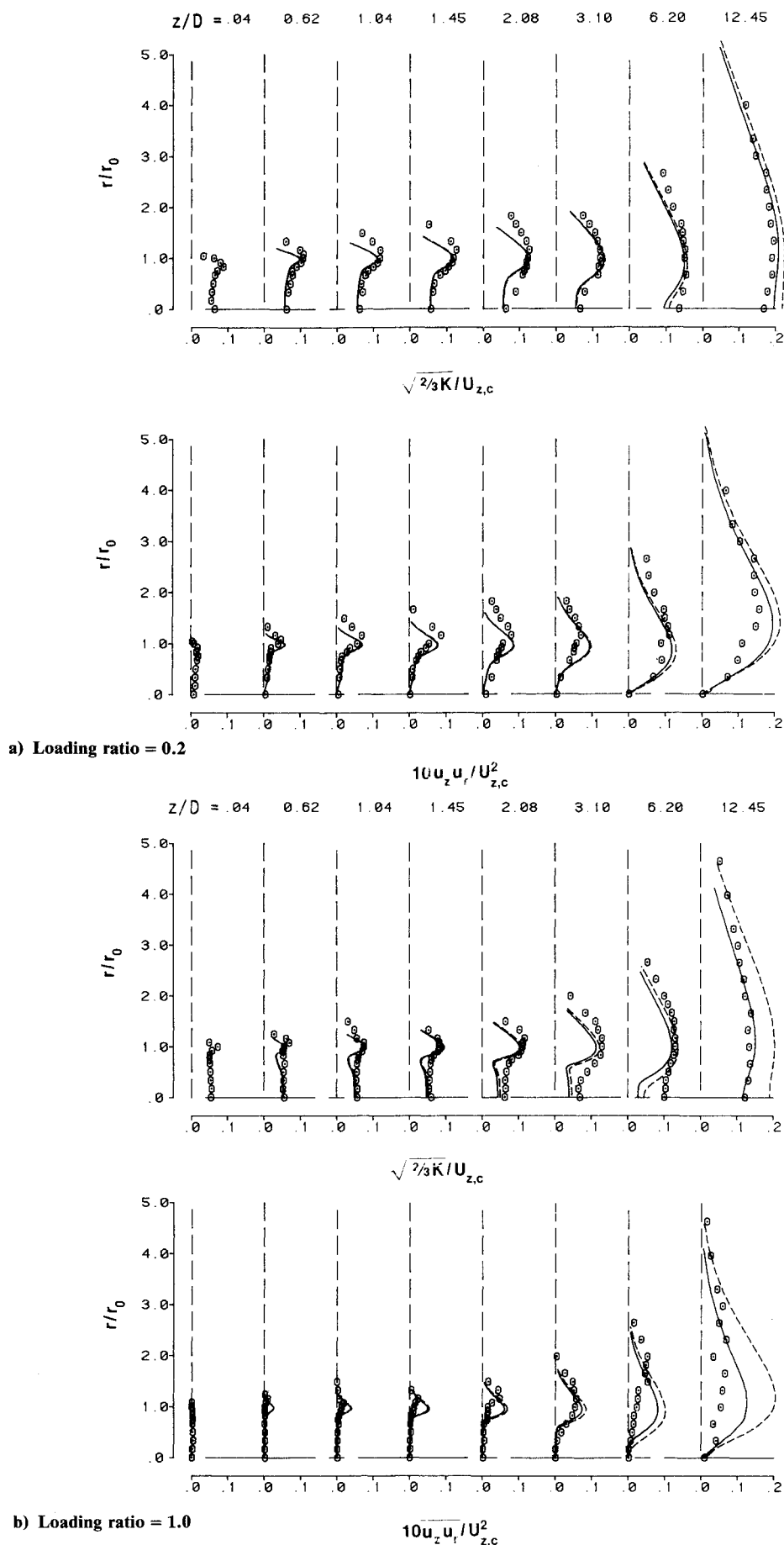
Fig. 13   Effect of single-phase and two-phase turbulence models on gas phase turbulence kinetic energy and shear stress for the two loading ratios, LR = 0.2 and 1.0; - - - two-phase model, —— single-phase model.

To see how the particles modulate the turbulence structure, distributions of turbulence kinetic energy and shear stress that are shown in Fig. 11 can be compared with the corresponding quantities of single-phase values illustrated in Fig. 4. At $z/D = 12.45$, local turbulence intensity is reduced from 20% to 12% at the centerline, which corresponds to a reduction of about 40% of the single-phase value. This turbulence modulation is caused mainly by the fluctuating relative velocity between the particles and the carrier phase. Particles generally cause a reduction in the gas turbulence and an increase in the dissipation rate of that energy. This turbulence attenuation reaches its maximum value at a certain mass loading ratio, when the particle relaxation time becomes very large compared with the gas Lagrangian time scale. The performance of the turbulence model for two-phase flows, which considers this physical phenomenon, is very good compared with the data in Figs. 11 and 12.

Figure 13 corresponds to measurements of the gas kinetic energy and shear stress at the two loadings and shows the predictions with the single-phase K-ϵ model and its version for two-phase flows.[17] In the latter, the turbulence modulation is simulated by introducing extra terms in the turbulence kinetic energy and its dissipation rate equations. Figure 13 shows that the single-phase model does not predict the turbulence modulation caused by the particles in the two cases. However, the two-phase flow model yields fairly good agreement with the data. This result confirms previous findings (e.g., Ref. 17) that the interaction between the gas and particles is indeed due to both relative mean and fluctuating motion between the two phases, and in some cases the turbulence modulation caused by the particles becomes equally important to the particle dispersion due to gas turbulence.

VI.   Conclusion

A detailed data set is presented for gas and particle mean and fluctuating velocity measurements and particle number density within the developing region of a particle-laden jet with 105 μm glass beads. The effect of particle mass loading ratio on the carrier-phase flow properties is investigated. The higher mass loading ratio (1.0) decreases the width and turbulence in the jet relative to the lower mass loading ratio (2.0). The variation in loading ratio also changes the nature of the inlet conditions.

The data have also been used to assess the accuracy of a two-phase transport model. The results show that stochastic treatment of the particles in conjunction with the two-phase turbulence model provides reasonable agreement with the data.

VII.   Acknowledgments

References

[1]Rajani, J. B., "Turbulent Mixing in a Free Air Jet Carrying Solid Particles," Ph.D. Thesis, Queen Mary College, London Univ., UK, 1972.

[2]Hetsroni, G. and Sokolov, M., "Distribution of Mass Velocity and Intensity of Turbulence in a Two-Phase Turbulent Jet," Journal of Applied Mechanics, Vol. 38, No. 2, June 1971, pp. 315-327.

[3]Laats, M. K. and Frishman, F. A., "Scattering of an Inert Admixture of Different Grain Size in a Two-Phase Axisymmetric Jet," Heat Transfer – Soviet Research, Vol. 2, 1970, pp. 7-12.

[4]Levy, T. and Lockwood, F. C., "Velocity Measurements in a Particle Laden Turbulent Free Jet," Combustion and Flame, Vol. 40, 1981, pp. 333-339.

[5]Popper, J., Abuaf, N., and Hetsroni, G., "Velocity Measurements in a Two-Phase Turbulent Jet," International Journal of Multiphase Flow, Vol. 1, 1974, pp. 715-726.

[6]Laats, M. K. and Frishman, F. A., "Assumptions Used in Calculating the Two Phase Jet," Fluid Dynamics, Vol. 5, No. 2, March-April 1970, pp. 333-338.

[7]Yuu, S., Yasukouchi, N., Hirowawa, Y., and Jotaki, T., "Particle Turbulent Diffusion in a Dust Laden Round Jet," AIChE Journal, Vol. 24, No. 3, May 1978, pp. 509-519.

[8]Modarress, D., Tan, H., and Elghobashi, S., "Two-Component LDA Measurement in a Two-Phase Turbulent Jet," AIAA Journal, Vol. 22, May 1984, pp. 624-630.

[9]Shuen, J.-S., Solomon, A. S. P., Zhang, Q. F., and Faeth, G. M., "Structure of Particle-Laden Jets: Measurements and Predictions," AIAA Journal, Vol. 23, No. 3, 1985, pp. 396-404.

[10]Melville, W. K. and Bray, K. N. C., "A Model of the Two-Phase Turbulent Jet," International Journal of Heat and Mass Transfer, Vol. 22, Feb. 1979, pp. 647-656.

[11]Pourahmadi, F. and Humphrey, J. A. C., "Modeling Solid-Fluid Turbulent Flows with Application to Predicting Erosive Wear," International Journal of Physicochemical Hydrodynamics, Vol. 4, No. 3, 1983, pp. 191-219.

[12]Elghobashi, S., Abou-Arab, T., Rizk, M., and Mostafa, A., "Prediction of the Particle-Laden Jet with a Two-Equation Turbulence Model," International Journal of Multiphase Flow, Vol. 10, No. 6, 1984, pp. 697-710.

[13]Crowe, C. T., "Review-Numerical Models for Dilute Gas-Particle Flows," ASME Journal of Fluids Engineering, Vol. 104, Sept. 1982, pp. 297-303.

[14]Gosman, A. D. and Ioannides, E., "Aspects of Computer Simulation of Liquid Fueled Combustors," AIAA Paper 81-0323, Jan. 1981.

[15]Dukowicz, J. K., "A Particle-Fluid Numerical Model for Liquid Sprays," Journal of Computational Physics, Vol. 35, No. 2, April 1980, pp. 229-253.

[16]Sirignano, W. A., "The Formulation of Spray Combustion Models: Resolution Compared to Droplet Spacing," Journal of Heat Transfer, Vol. 108, No. 3, Aug. 1986, pp. 633-639.

[17]Mostafa, A. A. and Mongia, H. C., "On the Modeling of Turbulent Evaporating Sprays: Eulerian Versus Lagrangian Approach," International Journal of Heat and Mass Transfer, Vol. 30, Dec. 1987, pp. 2583-2593.

[18]Boyson, F. and Swithenbank, J., "Spray Evaporation in Recirculating Flow," Seventeenth Symposium (International) on Combustion, The Combustion Inst., Pittsburgh, PA, 1979, pp. 443-453.

[19]Westbrook, C. K., "Three-Dimensional Numerical Modeling of Liquid Fuel Sprays," Sixteenth Symposium (International) on Combustion, The Combustion Inst., Pittsburgh, PA, 1976, pp. 1517-1526.

[20]Abbas, A. S., Koussa, S. S., and Lockwood, F. C., "The Prediction of the Particle Laden Gas Flows," Eighteenth Symposium (International) on Combustion, The Combustion Inst., Pittsburgh, PA, 1981, pp. 1427-1438.

[21]Smith, P. J., Fletcher, T. H., and Smoot, L. D., "Model for Pulverized Coal-Fired Reactors," Eighteenth Symposium (International) on Combustion, The Combustion Inst., Pittsburgh, PA, 1980, pp. 1285-1293.

[22]Bachalo, W. D. and Houser, M. J., "Phase Doppler Spray Analyzer for Simultaneous Measurements of Drop Size and Velocity Distributions," Optical Engineering, Vol. 23, No. 5, Sept.-Nov. 1984, pp. 583-590.

[23]Jackson, T. A. and Samuelsen, G. S., "Droplet Sizing Interferometry: A Comparison of the Visibility and Phase Doppler Techniques," Applied Optics, Vol. 26, June 1987, p. 2137.

[24]McDonell, V. G., Wood, C. P., and Samuelsen, G. S., "A Comparison of Spatially-Resolved Drop Size and Drop Velocity Measurements in an Isothermal Chamber and Swirl-Stabilized Combustor," Twenty-First Symposium (International) on Combustion, The Combustion Inst., Pittsburgh, PA, 1986, p. 685.

[25]Alexander, D. R., Wiles, K. J., Schaub, S. A., and Seeman, M. P., "Effects of Non-Spherical Drops on a Phase Doppler Spray Analyzer," SPIE Conference Proceedings, Vol. 573, Society of Photo-Optical Instrumentation Engineers, Bellingham, WA, 1985.

[26]McDonell, V. G. and Samuelsen, G. S., "Detailed Data Set: Two-Component Gas and Particle Velocity Statistics in a Particle-Laden Jet Flow," UCI Combustion Lab., Dept. of Mechanical Engineering, Univ. of California, Irvine, CA, Rept. ARTR 87-15, 1987.

[27]Faeth, G. M. and Samuelsen, G. S., "Fast Reaction Nonpremixed Combustion," *Progress in Energy and Combustion Science,* Vol. 12, No. 4, 1987, pp. 341–372.

[28]Clift, R., Grace, J. R., and Weber, M. E., *Bubbles, Drops, and Particles,* Academic, New York, 1978.

[29]Launder, B. E., Morse, A., Rodi, W., and Spalding, D. B., "The Prediction of Free Shear Flows: A Comparison of the Performance of Six Turbulence Models," Imperial College, London, England, Rept. TM/TN/19, 1975.

[30]Spalding, D. B., *GENMIX: A General Computer Program for Two-Dimensional Parabolic Phenomena,* Pergamon, Oxford, Eng-

land 1978.

[31]Shuen, J.-S., Chen, L. D., and Faeth, G. M., "Predictions of the Structure of Turbulent Particle-Laden Round Jets," *AIAA Journal,* Vol. 21, Nov. 1983, pp. 1483–1484.

[32]Bulzan, D. L., Shuen, J. S., and Faeth, G. M., "Particle-Laden Swirling Free Jets: Measurements and Predictions," AIAA Paper 87-0303, Jan. 1987.

[33]Mostafa, A. A. and Elghobashi, S. E., "A Two-Equation Turbulence Model for Jet Flows Laden with Vaporizing Droplets," *International Journal of Multiphase Flow,* Vol. 11, No. 4, July–Aug. 1985, pp. 515–533.